Pergamon

Electrochimica Acta, Vol. 43, Nos 5–6, pp. 549–561, 1998

Printed in Great Britain
PII: S0013-4686(97)00129-1
0013–4686/98 $19.00 + 0.00

The electrodeposition of mercury from aqueous Hg_2^{2+} ion-containing acid solutions on smooth and columnar-structured platinum electrodes

M. E. Martins, R. C. Salvarezza and A. J. Arvia*

Instituto de Investigaciones Fisiconquímicas Teóricas y Aplicadas (INIFTA) Sucursal 4, Casilla de Correo 16 (1900) La Plata, Argentina

(Received 30 October 1996; in revised form 10 March 1997)

Abstract—The electrodeposition of Hg on polycrystalline smooth and columnar structured Pt (cs-Pt) substrates was comparatively studied in acid solution at 298 K applying potentiodynamic techniques. The topography of both types of Pt electrodes was characterized by scanning tunneling microscopy. The use of cs-Pt substrates provides information about surface processes which are not easily detected on conventional smooth Pt. At moderate and high potential scan rates Hg electrodeposition under mass transport control on cs-Pt yields a non-equilibrium complex deposit consisting of 2d and 3d Hg domains, and Pt–Hg alloy coexisting with bare Pt domains at intercolumnar voids. The dynamics of these domains approaching equilibrium can be followed by conventional voltammetry. The kinetics of Hg penetration into bulk Pt results from a Hg atom shift to a position underlying the first layer of Pt atoms followed by a diffusion-controlled penetration into bulk Pt. The Hg atom diffusion coefficient into bulk Pt results in $D \cong 2 \times 10^{-17}$ cm^2 s^{-1}.

Key words: mercury electrodeposition, mercury underpotential electrodeposition, platinum electrode topography, mercury penetration into platinum, columnar-structured electrode

1. INTRODUCTION

The electrodeposition of Hg on Pt electrodes from Hg_2^{2+} ion-containing aqueous acid solutions has been investigated for a long time both in the underpotential (upd) and the overpotential deposition (opd) ranges including amalgam formation [1–7, 9, 10]. The Hg electrodeposition reaction on Pt involves the formation of Hg–Pt surface compounds [2–7] and bulk Hg on top of the modified electrode [6]. The maximum amount of upd Hg on Pt corresponds to a full monolayer (ML) surface coverage [6] yielding a square lattice Hg structure [1] which inhibits entirely the H-adatom electrosorption [6]. Otherwise, when the amount of deposited Hg exceeds the ML charge, Hg atoms can diffuse into bulk Pt to form either an alloy, or different intermetallic compounds [6–10]. In agreement with anodic stripping data on those Hg-films produced on Pt [2], thermogravimetric data from Hg vapor deposited on Pt have demonstrated [11–13] that some amount of Hg always remains as a surface compound which can only be desorbed at 160°C [11], whereas Pt–Hg intermetallic compounds decompose at even higher temperatures, as it was found that Hg still remains on Pt up to 800°C [12].

For a number of metal ML and multilayer electroformation on different Pt single crystal faces, polycrystalline Pt, platinized Pt and columnar Pt electrodes [1–7, 9, 10, 14–25], it has been found that the initial stages of these processes depend on the crystallography and topography of the substrate. If such a situation can be proved for Hg electrodeposition on Pt, then it can render an explanation for some rather different results reported in the literature for this system [1–7, 9, 10, 25].

This work refers to the influence of the Pt surface topography on Hg upd and opd from Hg_2^{2+} ion-containing aqueous acid solutions when the same type of experiments are run on both smooth and columnar-structured Pt electrodes. The surface of these electrodes behaves as a fractal [26] surface, a

*Author to whom correspondence should be addressed.

fact which is particularly interesting to enhance the contribution of surface processes playing a part in the overall electrochemical reaction such as Hg surface atom diffusion and Hg penetration into bulk Pt. The extent of these processes determines whether the inhibition of the H- and O-electrosorption reactions on Pt due to Hg electrodeposition is either partial or complete. Furthermore, depending on the roughness factor for columnar-structured electrodes under the usual voltammetric conditions and on the extent of the Hg electrodeposition reaction, a cs-Pt electrode in contact with the electrolyte solution may consist of Hg(upd), Hg(opd), Hg–Pt and Pt coexisting domains which are detectable for a relatively long time.

2. EXPERIMENTAL

Two types of Pt working electrodes, namely, smooth polycrystalline (pc) Pt (0.06 cm^2 in geometric area) and columnar-structured Pt (cs-Pt) were employed. Each working electrode was mounted into a glass electrochemical cell together with a Pt gauze counter electrode, and a reversible hydrogen electrode (*rhe*) in the working solution as reference electrode. The following working aqueous solutions were employed: x M $Hg_2(NO_3)_2 + 0.5$ M $HClO_4$ ($10^{-4} \leqslant x \leqslant 10^{-3}$), and plain 0.5 M $HClO_4$ as blanks. Solutions were prepared from p.a. quality chemicals and Milli-Q* water. Runs were performed at 25°C under N_2 saturation at atmospheric pressure.

The preparation technique for cs-Pt electrodes was the same as that described elsewhere [27, 28]. As has been concluded from scanning tunneling microscopy (STM) [29, 30], ellipsometry [31], ultraviolet and visible electroreflectance spectroscopy [32], and electrochemical data [20, 21, 23, 25, 33–37], the columnar microstructure of cs-Pt consists of an average column height in the range 10–10,000 nm, a void-to-filled volume ratio of about 0.5, and columns and intercolumnar voids about 10 nm in average diameter (Fig. 2).

Each cs-Pt electrode behaves as a rough polycrystalline Pt electrode with an almost constant distribution of crystallographic orientations, regardless of the magnitude of the roughness factor (R), at least in the range $1 \leqslant R \leqslant 10^3$ [26, 27]. These electrodes attain a stable value of R after being immersed in aqueous 1 M H_2SO_4 for 24 h [20, 21, 23–37]. The value of R was defined as the $(Q_H)_R/(Q_H)_I$ ratio, where $(Q_H)_R$ and $(Q_H)_I$ are the H-atom electrodesorption voltammetric charge for cs-Pt and smooth pc-Pt electrodes, respectively, both measured in aqueous 1 M H_2SO_4 under the same voltammetric conditions [26, 38]. Values of R which were checked initially and at the end of each experiment were comprised in the range $10 \leqslant R \leqslant 200$. The characterization of the cs-Pt electrode was made by *ex situ* STM imaging with a Nanoscope III STM operating in air. STM tips were made from Pt-Ir Nanotips. STM measurements were performed using a 0.05–0.10 bias voltage with the tip (+) at 1–2 nA constant current. Different tips were used to discard occasional artifacts caused by the tip geometry. STM images were presented as raw data with plane removal only.

Single sweep (STPS-I) and repetitive (RTPS-I) voltammetric techniques were applied from the cathodic $E_{sc} = 0.05$ V, to the anodic switching potential $E_{sa} = 1.45$ V, in the potential sweep rate range $0.005\ \text{V s}^{-1} \leqslant v \leqslant 0.1\ \text{V s}^{-1}$. Besides, STPS runs including a potential holding at E_h set in the range $0.05\ \text{V} \leqslant E_h \leqslant 1.40\ \text{V}$ (STPS-II) were also performed. In this case, the potential holding was included in the negative-going potential scan for a time t_h in the range $10\ s \leqslant t_h \leqslant 600$ s. Subsequently, the potential scan was continued from E_h down to E_{sc} at 10 V s^{-1}, and the reversal scan from E_{sc} to E_{sa} was made at 0.1 V s^{-1}.

Finally, repetitive voltammetric runs (RTPS-II) were made in the range $0.02\ \text{V s}^{-1} \leqslant v \leqslant 0.10\ \text{V s}^{-1}$ by setting E_{sa} in the range $0.75\ \text{V} \leqslant E_{sa} \leqslant 1.45$ V, and E_{sc} in the range $0.05\ \text{V} \leqslant E_{sc} \leqslant 0.8$ V.

3. RESULTS AND INTERPRETATION

3.1. STM imaging of Pt substrates

The STM image of a conventionally prepared smooth pc-Pt ($100 \times 100\ nm^2$) (Fig. 1(a)), shows flat terraces about 30 nm in width with a typical corrugation of the order of 0.2 nm. The cross section analysis (Fig. 1(b)) reveals that these terraces are separated by steps of about 3 atoms in height forming well-defined angles.

The STM images ($100 \times 100\ nm^2$ and $30 \times 30\ nm^2$) of a cs-Pt electrode ($R \cong 30$) (Fig. 2(a), (b)) show a rough topography on two scales, namely, a broad columnar structure 10–20 nm in average size, and a fine cluster structure within each column, each cluster being about 2–5 nm in average size. The cross section analysis (Fig. 2(c)) shows that intercolumnar voids are 10 nm in average size, although smaller surface irregularities can be also observed.

3.2. Reference voltammetry data from smooth pc Pt

STPS-I voltammograms resulting from a pc-Pt electrode in aqueous 0.5 M $HClO_4 + 10^{-4}$ M $Hg_2(NO_3)_2$ at $v = 0.1\ \text{V s}^{-1}$ covering from $E_{sa} = 1.45$ V to $E_{sc} = 0.3$ V (Fig. 3(a)), show a cathodic current peak (Ic) at 0.75 V including a shoulder (II′c) which has been assigned to the simultaneous O-electrodesorption and initiation of Hg upd [10], followed by a current plateau (IIIc) extending from 0.35 V to 0.05 V. Both the shoulder (II′c) and current plateau (IIIc) have been related to Hg opd [6]. Otherwise, the reverse potential scan initially involves a net cathodic limiting current (IIIa) followed by a small anodic current peak (IIa) at 0.66 V, which has been associated with the electrodissolution of bulk Hg. Later, a complex anodic peak (Ia) at 1.07 V which has been

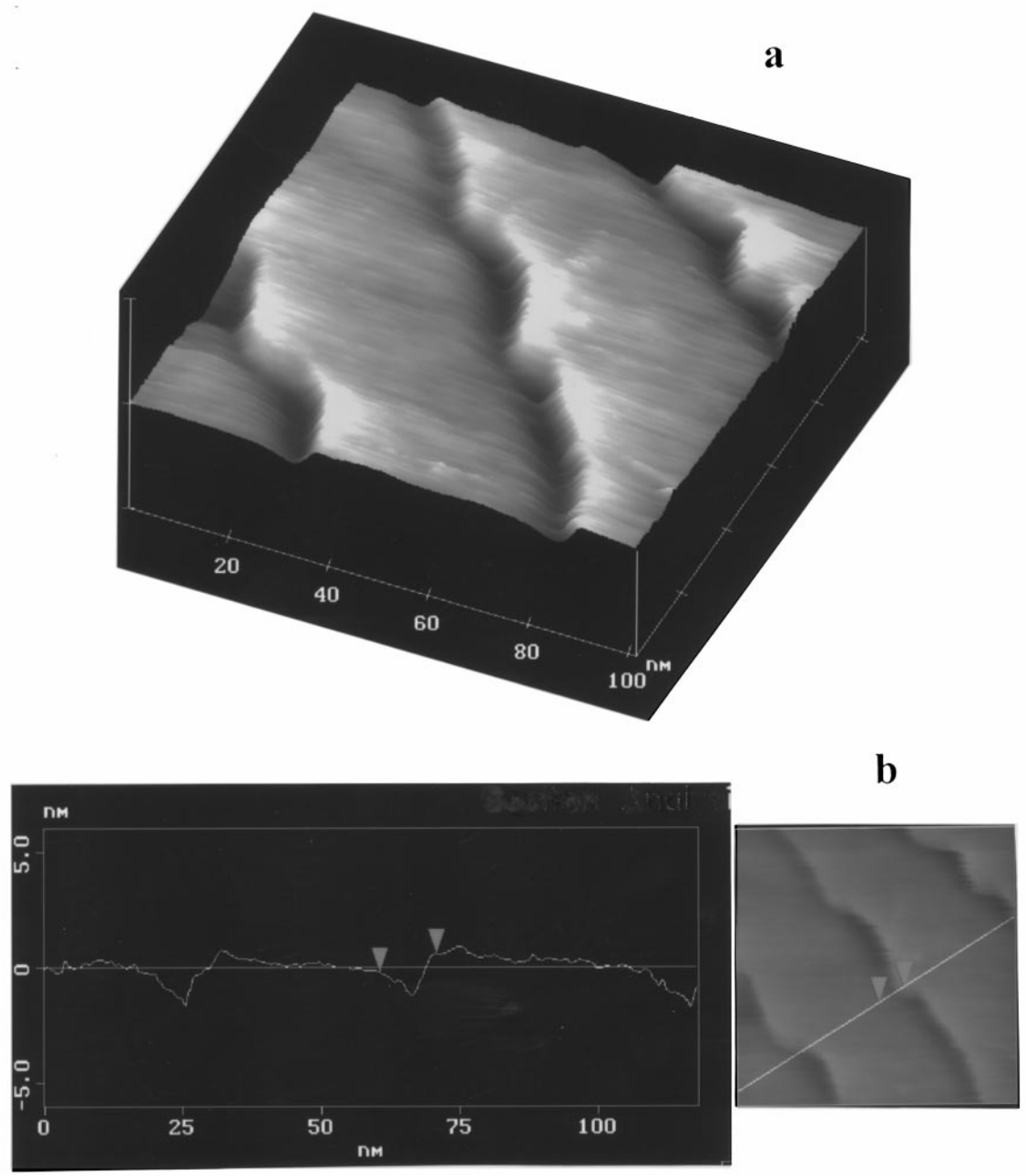

Fig. 1. (a) Constant current 100 × 100 nm^2 STM image of a smooth Pt electrode; (b) cross section of the STM image shown in Fig. 1(a). Terraces separated by steps about 3 atoms in height can be seen.

assigned to the overlapped stripping of Hg upd and O-electroadsorption can be observed [6, 10].

The above description can be improved by considering those RTPS-II voltammograms in which E_{sa} was either decreased or increased stepwise. Thus, for $E_{sc} = 0.03$ V and $v = 0.1$ V s^{-1}, as E_{sa} is decreased (Fig. 3(b)), both peak Ic at 0.75 V (Hg upd) and peak IIc at 0.64 V (Hg opd) can be distinguished. In these runs the progressive inhibition of O-electroadsorption can also be observed, making the definition of peaks IIa and IIc much clearer. These peaks have been related to Hg bulk electrodeposition and Hg electrodissolution, respectively [6]. In fact, they are located near $E_r = 0.674$ V, the reversible potential of the Hg/Hg_2^{2+} redox couple calculated for our system [39–41].

Furthermore, the longer the repetitive potential scanning between $E_{sc} = 0.03$ V and $E_{sa} = 1.18$ V (Fig. 3(b)), *ie* within the potential range of the Hg/Hg_2^{2+} redox couple, the greater the increase in height of peaks IIa and Ia. Subsequently, as E_{sa} is increased from 1.18 V upwards (Fig. 3(c), (d)), it

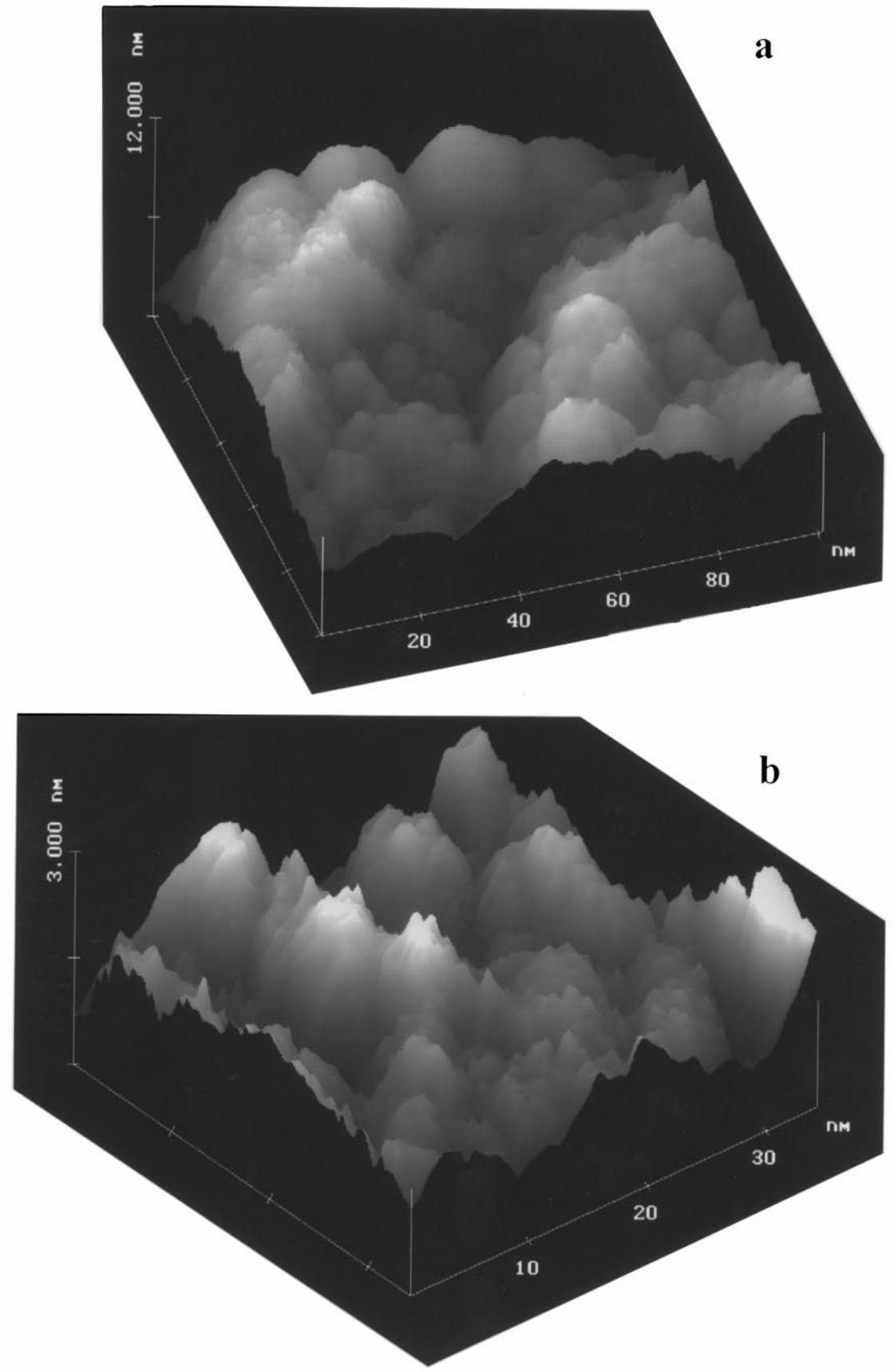

Figure 2

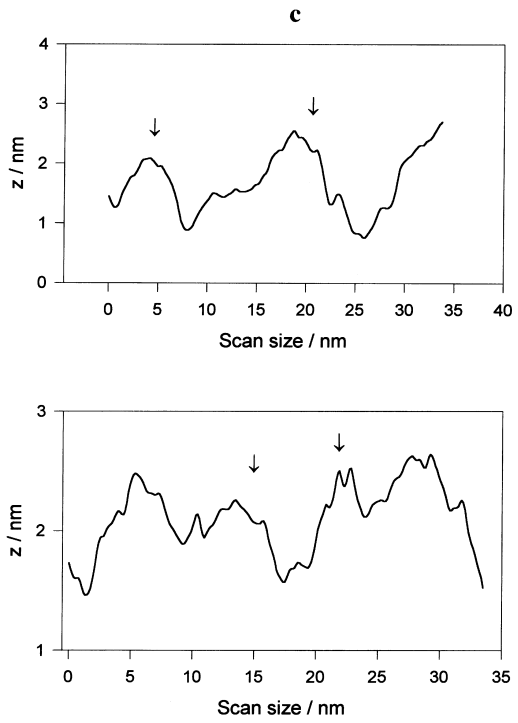

Fig. 2. (a) Constant current 100×100 nm^2 STM image of a cs-Pt electrode ($R = 30$); (b) 30×30 nm^2 STM image showing the presence of small clusters on the column surface; (c) cross section of the STM image shown in Fig. 1(b).

results in a slow decrease in peak IIa, and the splitting of peak Ia into peak I′a at 1.16 V, and peak I″a at 1.24 V. Peak I′a has been related to the anodic stripping of the Hg 2d layer on Pt, whereas peak I″a has been attributed to O-electroadsorption [6, 10]. However, by potential cycling for $E_{sa} = 1.43$ V, the voltammogram shown in Fig. 3(a) is recovered as indicated by the arrows in Fig. 3(d).

3.3. Voltammetry data from cs-Pt

Voltammetry data resulting from cs-Pt electrodes were obtained applying the different potential routines by changing systematically v, E_{sc}, E_{sa}, E_h, t_h, and R.

The voltammogram for Hg electrodeposition/anodic stripping on cs-Pt under routine STPS-I is substantially different to that observed on pc Pt. For $R = 30$ and $x = 10^{-4}$ the voltammogram run from E_{sa} downwards at $v = 0.005$ V s^{-1} (Fig. 4(a)) shows the cathodic current peak Ic followed by a limiting current covering the range of 0.50 V to 0.03 V. These current contributions are due to Hg opd overlapping to some extent H-electroadsorption undergoing in the range 0.35 V to 0.03 V. The reverse potential scan still shows the Hg opd limiting current and H-electrodesorption overlapping current, at least in the range 0.03 V to 0.50 V. Then, peak IIa corresponds to bulk Hg anodic stripping, and finally, from 0.8 V to 1.45 V, a complex current contour involving O-electroadsorption at free Pt sites (peak Ia), Hg 2d layer anodic stripping (peak I′a), and presumably, Hg dealloying (peak I″a) can be seen. A similar run made at $v > 0.005$ V s^{-1} (Fig. 4(b)) shows an enhancement of the conjugated peaks related to H-electrosorption and the absence of peak IIa. These results reveal that under the voltammetric conditions described in Fig. 4(b), Hg opd on cs-Pt electrodes is largely hindered.

To emphasize the influence of R on Hg electrodeposition under routine RTPS-II ($E_{sc} = 0.02$ V and $E_{sa} = 1.45$ V) runs were also made at 0.1 V s^{-1} $R = 150$ and $x = 10^{-4}$ M. In this case, the voltammogram in the positive potential direction (Fig. 4(c)) shows that H-electroadsorption in the range 0.02 V to 0.35 V takes place on a Pt surface which is partially inhibited by Hg adatoms, a linear current increase in the range 0.36 V to 0.76 V followed by a current plateau due to the early stages of O-electroadsorption, a complex current peak at 1.19 V involving the anodic stripping of Hg, and finally, an anodic current contribution which steadily decreases as E_{sa} is reached. The reverse scan displays an asymmetric cathodic peak at 0.75 V accompanied by a shoulder at 0.9 V, which is related to the O-atom electrodesorption and Hg upd, respectively. Finally, in the range 0.35 V to 0.02 V, H-electroadsorption takes place. It should be noted that voltammograms run under routine STPS-I at constant v and increasing R exhibit almost the same features as those described above for a constant R and increasing v. From these

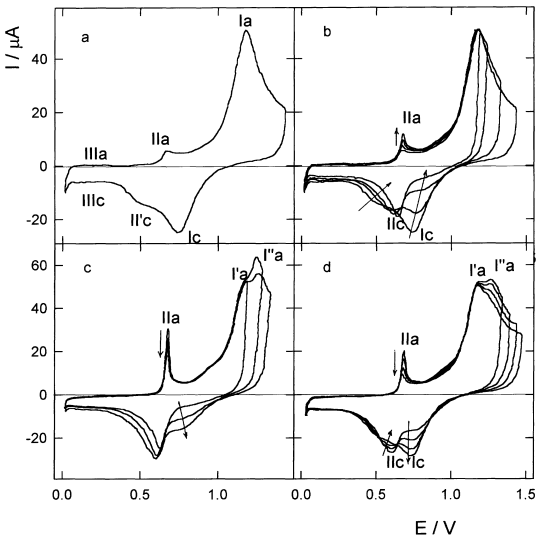

Fig. 3. Voltammograms related to the electrodeposition and anodic stripping of Hg on a pc-Pt electrode in 0.5 M $HClO_4 + 10^{-4}$ M $Hg_2(NO_3)_2$ at $v = 0.1$ V s^{-1}. (a) STPS-I voltammogram covering from $E_{sa} = 1.45$ V to $E_{sc} = 0.03$ V; (b) RTPS-II voltammograms with E_{sa} decreasing stepwise; (c) (d) RTPS-II voltammograms with E_{sa} increasing stepwise.

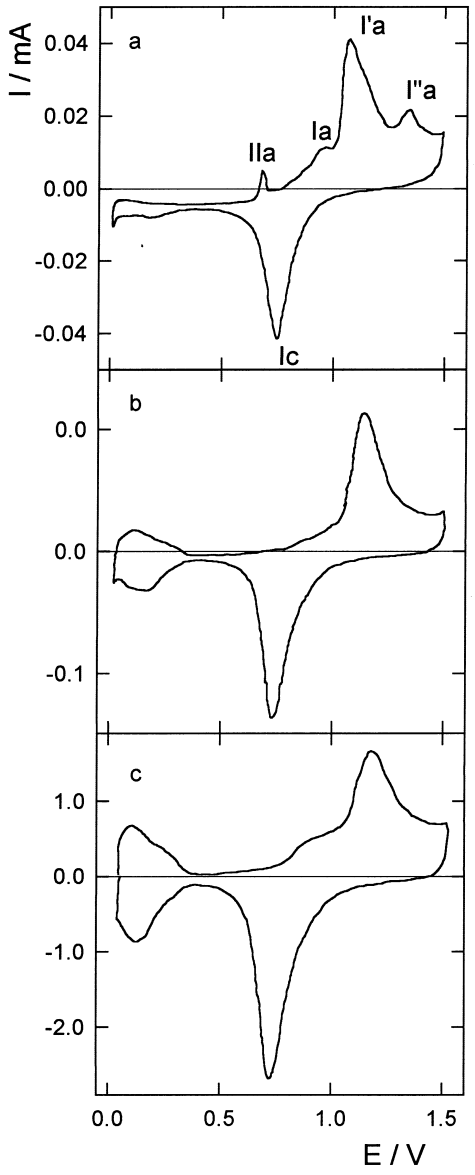

Fig. 4. Voltammograms related to the electrodeposition and anodic stripping of Hg on a cs-Pt electrode in 0.5 M $HClO_4 + 10^{-4}$ M $Hg_2(NO_3)_2$. (a) $v = 0.005$ V s^{-1}, $R = 30$; (b) $v = 0.02$ V s^{-1}, $R = 30$; (c) $v = 0.1$ V s^{-1}, $R = 150$.

experiments it can be concluded that at least within the range of variables covered in this work, Hg opd on cs-Pt is limited to some extent, the relative contribution of this reaction as compared to the H- and O-electrosorption decreases when either R or v is increased.

Additional features of those processes involved in Hg deposition on cs-Pt were obtained from those runs made for $R = 70$ and $x = 10^{-3}$, at 0.02 V s^{-1} applying routine STPS-I. Accordingly, once a repetitive voltammogram had been obtained (Fig. 5(a)), the value of E_{sa} was either decreased or increased stepwise. On decreasing E_{sa} from 1.54 V to 1.34 V, the voltammogram shows competitive current contributions (peaks Ia, I′a, Ic and I′c) related to Hg anodic stripping/cathodic deposition, and O-electrosorption reactions (Fig. 5(b)). Otherwise, voltammograms resulting from E_{sa} set in the range $1.14\ \text{V} \leqslant E_{sa} \leqslant 1.34\ \text{V}$ (Fig. 5(b)) exhibit the disappearance of O-electrosorption; the enhancement of Hg electrodeposition current peaks at 0.98 V (peak I′c) and 0.65 V (peak IIc), corresponding to the Hg(II)⇒Hg(I) and Hg(I)⇒Hg(0) reaction, respectively; the incipient anodic stripping of bulk Hg at

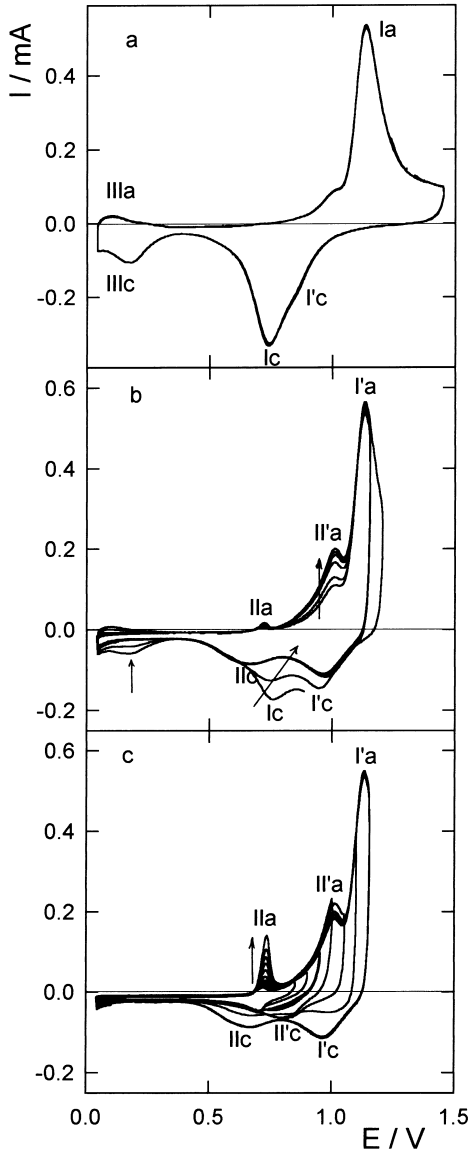

Fig. 5. Voltammograms related to the electrodeposition and anodic stripping of Hg on a cs-Pt electrode ($R = 70$) in 0.5 M $HClO_4 + 10^{-3}$ M $Hg_2(NO_3)_2$ at $v = 0.02$ V s^{-1}. (a) STPS-I voltammogram covering from $E_{sa} = 1.45$ V to $E_{sc} = 0.03$ V; (b) (c) RTPS-II voltammograms with E_{sa} decreasing stepwise.

0.7 V (peak IIa); the stripping of the outer second Hg layer yielding Hg(II) at 1 V (peak II′a); the stripping of the first Hg monolayer at 1.14 V (peak I′a) [6]. Further cycling in the range $E_{sc} = 1.14$ V to $E_{sa} = 1.34$ V (Fig. 5(b)) results in the stabilization of peak I′a and the progressive increase in peak II′a. Subsequently, the stepwise decrease in E_{sa} in the range $0.84\ \text{V} \leqslant E_{sa} \leqslant 1.10\ \text{V}$ (Fig. 5(c)), clearly shows current peaks II′a and II′c related to the electrodeposition/anodic stripping of the second Hg layer, and current peaks IIa and IIc associated with the electroformation/anodic dissolution of bulk Hg.

On the other hand, a potential cycling in the range $E_{sc} = 0.02$ V to $E_{sa} \geqslant 0.80$ V was made (Fig. 5(c)) to enhance Hg opd and to assist Pt–Hg alloy formation. Thus, voltammograms resulting for E_{sa} in the range $0.84\ \text{V} \leqslant E_{sa} \leqslant 1.05\ \text{V}$ (Figs 5(c), 6(a)), show a continuous increase in current related to Hg opd and its anodic stripping, and an almost complete inhibition of H-electrosorption as the cs-Pt surface becomes thoroughly covered by Hg atoms. However, when E_{sa} is changed stepwise from 1.05 V upwards (Fig. 6(b)), from the decrease in the height of peak IIa and the increasing anodic current related to the formation of Hg(I) and Hg(II) species, the gradual

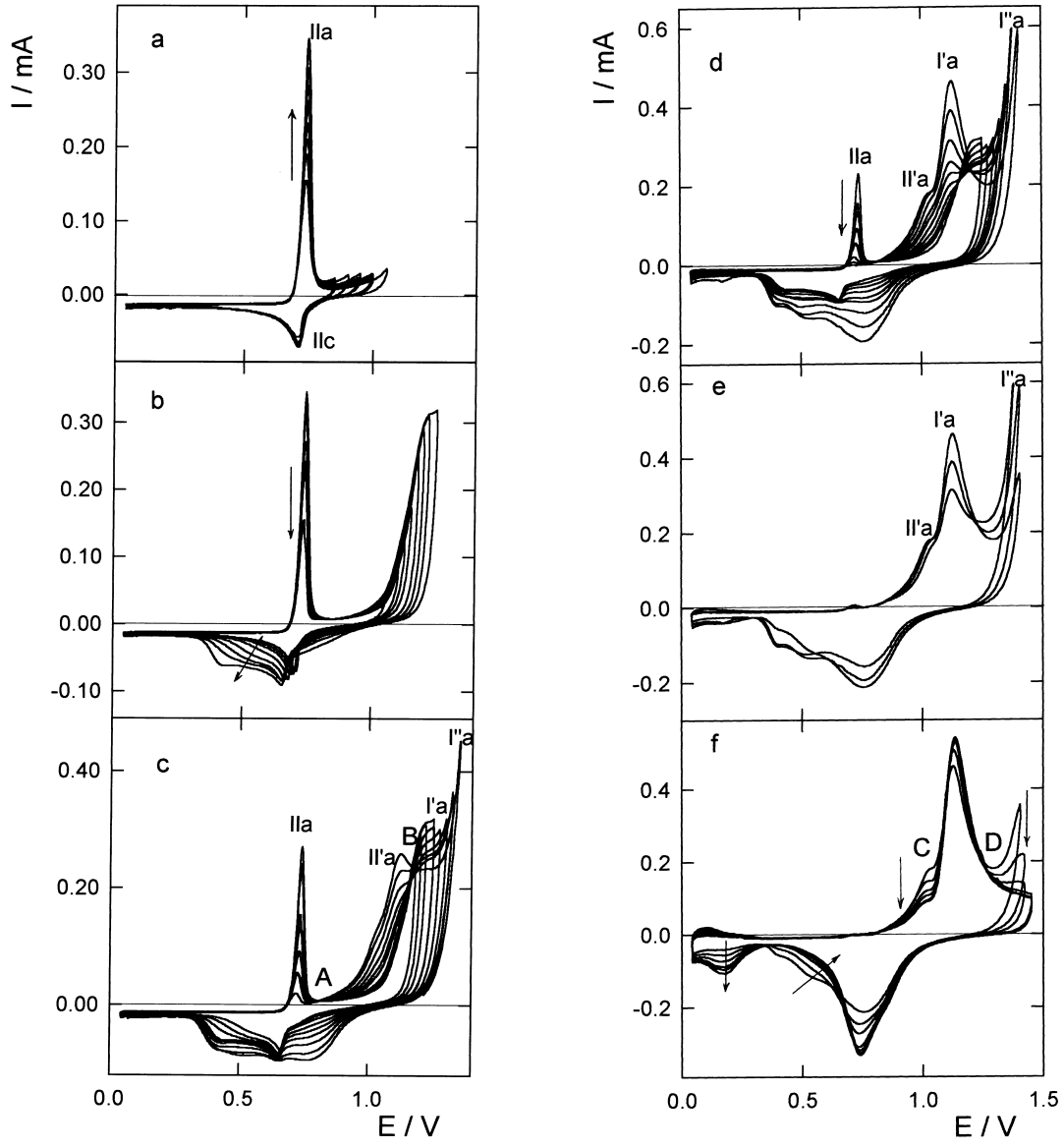

Fig. 6. Voltammograms related to the electrodeposition and anodic stripping of Hg on a cs-Pt electrode ($R = 70$) in 0.5 M $HClO_4 + 10^{-3}$ M $Hg_2(NO_3)_2$ at $v = 0.02\ \text{V s}^{-1}$. RTPS-II voltammograms with $E_{sc} = 0.02$ V and E_{sa} increasing stepwise. (a) $0.84\ \text{V} \leqslant E_{sa} \leqslant 1.05$ V; (b) $1.05\ \text{V} \leqslant E_{sa} \leqslant$; (c) $1.20\ \text{V} \leqslant E_{sa} \leqslant 1.32$ V; (d) $1.24\ \text{V} \leqslant E_{sa} \leqslant 1.39$ V; (e) $1.36\ \text{V} \leqslant E_{sa} \leqslant 1.39$ V; (f) $1.40\ \text{V} \leqslant E_{sa} \leqslant 1.45$ V.

electrodissolution of bulk Hg followed by the incipient stripping of outer layer Hg atoms can be deduced. Those species are electroreduced in the reverse potential scan (Fig. 6(b)). Likewise, for E_{sa} set in the range $1.20\ V \leqslant E_{sa} \leqslant 1.32\ V$ (Fig. 6(c)), voltammograms show again the stripping of bulk Hg (peak IIa), and the anodic stripping of the second (peak II′a) and first Hg layer (peak I′a). Accordingly, isopotentials at 0.82 V (A) and 1.16 V (B) (Fig. 6(c)) resulting from the decrease in the current contribution of both peaks I′a and IIa and the increase in that related to peak II′a can then be defined.

The enhancement of peak I″a related to the electrooxidation of subsurface Hg species can be seen by increasing E_{sa} from 1.3 V upwards (Fig. 6(c)–(e)). In this case, the increase in peaks I′a and II′a can also be observed, although the height of peak II′a reaches a maximum at the expense of peak I″a. Moreover, setting E_{sa} in the range $1.40\ V \leqslant E_{sa} \leqslant 1.45\ V$ (Fig. 6(f)) results in the decrease in peaks II′a and I″a, and the increase in peak I′a up to its maximum value, and then isopotentials C and D can be distinguished (Fig. 6(f)). Subsequently, a repetitive potential scan from $E_{sc} = 0.02$ V to $E_{sa} = 1.45$ V at $v = 0.02\ V\ s^{-1}$ leads to a stabilized voltammogram which corresponds to a cs-Pt electrode partially covered by a Hg atom submonolayer.

From the above results it can be concluded that depending on E_{sa}, a Hg film ranging from a submonolayer to several monolayer average thickness can be formed on cs-Pt, and Hg atoms can also penetrate into bulk Pt. Accordingly, Hg(I) and/or Hg(II) species produced for the potential scan in the positive direction are electrodeposited in the subsequent reverse scan on a cs-Pt surface either entirely (Fig. 6(a)–(c)) or partially covered by Hg atoms (Fig. 6(d)–(f)). In these cases, the voltammetric features of the negative-going potential scans depend considerably on E_{sa}.

3.3.1. *The evaluation of voltammetric charges*. The electrodeposition of Hg on cs-Pt depends on R, v, E_{sc}, E_{sa}, E_h, t_h, and x. Quantitative data on the effect of E_h and t_h on the Hg anodic stripping were obtained for $70 \leqslant R \leqslant 145$, $10^{-4} \leqslant x \leqslant 10^{-3}$, $E_{sc} = 0.05$ V and $E_{sa} = 1.45$ V, with the application of routine STPS-II including a potential holding at E_h. In this case, the electrodeposition of Hg was previously made for $30\ s \leqslant t_h \leqslant 240\ s$ at a potential set in the range $0.05\ V \leqslant E_h \leqslant 1.45\ V$. This range of E_h covered from the early stages of Hg electrodeposition to bulk Hg formation including Pt–Hg alloying (Fig. 7(a)–(c)). The apparent charge densities calculated from voltammetric data on Hg electrodeposition (q_{Hg}), H-atom electrosorption (q_H) and the O-atom electrosorption (q_O) are both E_h- and t_h-dependent.

The value of q_H was obtained in the range $0.03\ V \leqslant E \leqslant 0.35\ V$; the value of q_{Hg+O}, related to the O-atom electroadsorption and anodic stripping of Hg upd, and occasionally, the anodic stripping of the Hg/Pt alloy, was estimated in the range

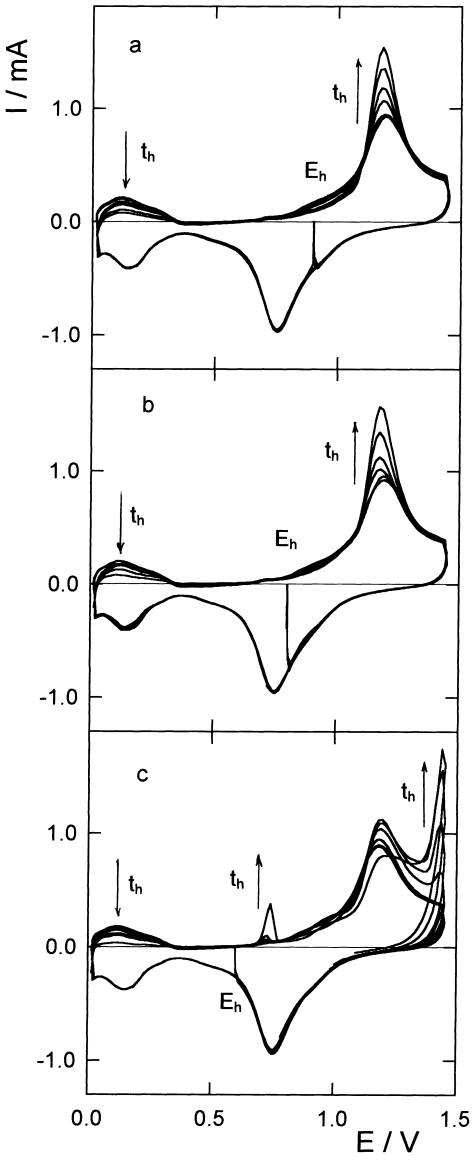

Fig. 7. Voltammograms related to the electrodeposition and anodic stripping of Hg on a cs-Pt electrode ($R = 70$) in $0.5\ M\ HClO_4 + 10^{-3}\ M\ Hg_2(NO_3)_2$ at $v = 0.1\ V\ s^{-1}$ under the application of routine STPS-II including a potential holding at E_h for $t_h = 30$, 60, 120, 240 s. (a) $E_h = 0.9$ V; (b) $E_h = 0.6$ V; (c) $E_h = 0.5$ V.

$0.75\ V \leqslant E \leqslant 1.45\ V$. The value of q_{Hg}, was calculated as $q_{Hg+O} - q_O$, and the value of q_O was estimated indirectly from the value of q_H, considering that it reflects the number of sites at cs-Pt available for O-electroadsorption. Then, $q_{Hg} = q_{Hg+O} - 2\ q_H$.

The dependence of q_H and q_{Hg} on E_h (Fig. 8(a), (b)), defines three potential domains (I, II and III), which determine the potential ranges in which Hg and upd and Hg opd reactions compete with the H- and O-electrosorption. Otherwise, when E_h is within the range $1.10\ V \leqslant E_h \leqslant 1.45\ V$ and $30\ s \leqslant t_h \leqslant 240\ s$

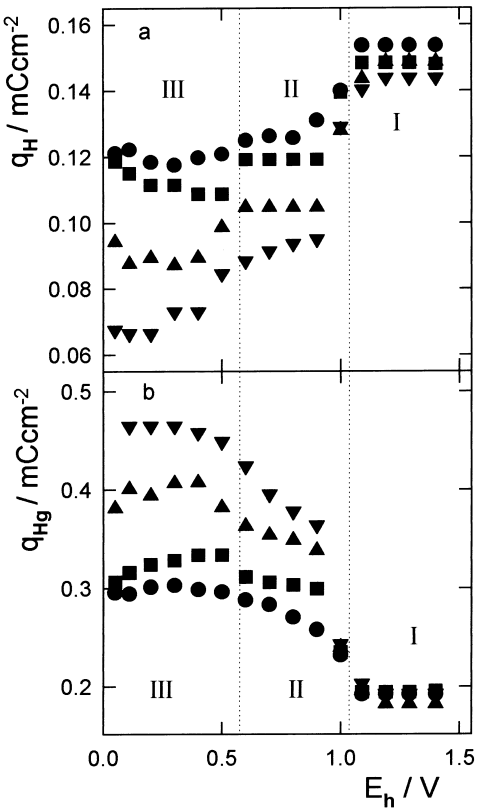

Fig. 8. (a) q_H vs E_h plot; (b) q_{Hg} vs E_h plot. Data derived from routine STPS-II applied to a cs-Pt electrode ($R = 70$) in 0.5 M $HClO_4 + 10^{-3}$ M $Hg_2(NO_3)_2$ at $v = 0.1$ V s^{-1} and 0.05 V $\leqslant E_h \leqslant$ 1.45 V and 30 s $\leqslant$ 240 s. $t_h = 30$ s (●), 60 s (■), 120 s (▲), 240 s (▼).

(Fig. 8(a), (b)), both q_H and q_{Hg} become almost independent of E_h, their values resulting in $q_H \cong 150 \pm 8$ μC cm^{-2} and $q_{Hg} \cong 188 \pm 10$ μC cm^{-2} (domain I in Fig. 8(a), (b)). Values of q_H and q_{Hg} derived for $E_h \gg E_r$ indicate that in this case an amount of Hg smaller than that expected for single Hg ML was electrodeposited. Seemingly, the cs-Pt surface became only partially accessible to the discharge of Hg_2^{2+} ions, whereas both the O- and H-electroadsorption reactions underwent at the remaining surface.

As E_h is shifted negatively within the range 0.9 V $\leqslant E_h \leqslant$ 1.1 V, *ie*, covering the Hg upd region, unlike to q_{Hg}, q_H decreases sharply because the cs-Pt surface resulting from O-atom electrodesorption becomes immediately occupied by electrodeposited Hg. Nevertheless, for $E_h \gg E_r$ a fraction of the cs-Pt surface remains covered by O atoms, whereas for $E_h \Rightarrow E_r$, the Pt surface becomes progressively occupied by Hg atoms, as can be concluded from the slight increase in q_{Hg} (Fig. 8(b)). In this case, the value of q_H remains almost constant, irrespective of E_h.

Finally, for $E_h < E_r$, the value of q_{Hg} increases substantially with E_h, although for $E_h < 0.1$ V, a

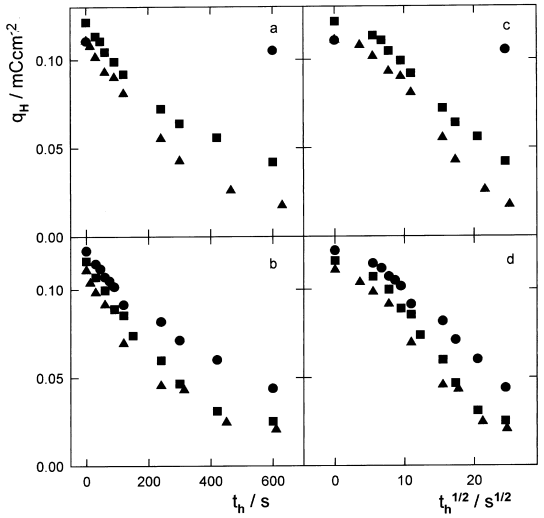

Fig. 9. q_H vs t_h plots and q_H vs $t_h^{1/2}$ plots. Data derived from routine STPS-II applied to a cs-Pt electrode ($R = 145$) in 0.5 M $HClO_4 + 10^{-4}$ M $Hg_2(NO_3)_2$ at $v = 0.1$ V s^{-1} and 0.05 V $\leqslant E_h \leqslant$ 1.45 V and 30 s $\leqslant t_h \leqslant$ 240 s. (a), (c) $E_h = 0.6$ V (▲), 0.8 V (■), 1.0 V (●); (b), (d) $E_h = 0.5$ V (▲), 0.7 V (■), 0.9 V (●).

slight increase in q_H, and correspondingly a decrease in q_{Hg}, can be observed.

Voltammetric data derived from routine STPS-II for E_h set in the range 0.5 V $\leqslant E_h \leqslant$ 1.0 V become t_h-dependent. Thus, for $0 \leqslant t_h \leqslant 120$ s, a linear q_H vs t_h plot is approached (Fig. 9(a), (b)), but for $t_h > 120$ s a trend to a q_H vs $t_h^{1/2}$ linear plot can be observed (Fig. 9(c), (d)), indicating a possible

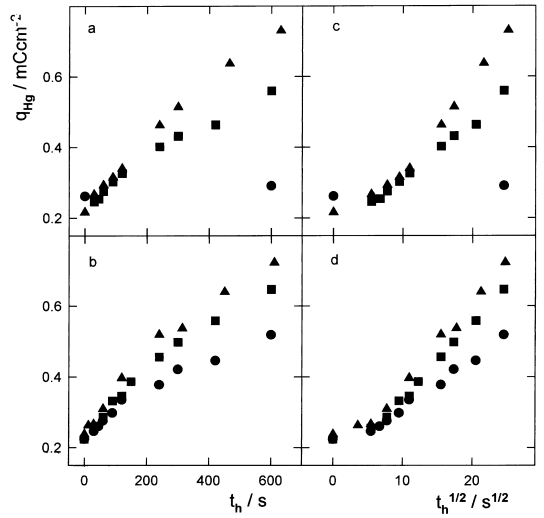

Fig. 10. q_{Hg} vs t_h plots and q_{Hg} vs $t_h^{1/2}$ plots. Data derived from routine STPS-II applied to a cs-Pt electrode ($R = 145$) in 0.5 M $HClO_4 + 10^{-4}$ M $Hg_2(NO_3)_2$ at $v = 0.1$ V s^{-1} and 0.05 V $\leqslant E_h \leqslant$ 1.45 V and 30 s $\leqslant t_h \leqslant$ 240 s. (a), (c) $E_h = 0.6$ V (▲), 0.8 V (■), 1.0 V (●); (b), (d) $E_h = 0.5$ V (▲), 0.7 V (■), 0.9 V (●).

change of the kinetics in the electrochemical reaction.

Similarly, for values of E_h comprised in the range $0.5\ V \leqslant E_h \leqslant 0.9\ V$, the q_{Hg} vs t_h plots (Fig. 10(a), (b)) show a linear portion with a E_h-independent common slope extending from 0 to 120 s, and $q_{Hg} \cong 220\ \mu C\ cm^{-2}$ at $t_h = 0$. This figure coincides with that derived from Hg anodic stripping data under routine RTPS-I. Conversely, q_{Hg} vs $t_h^{1/2}$ linear plots (Fig. 10(c), (d)) can be observed for $t_h > 120$ s, with slopes increasing as E_h is decreased.

Results obtained from the application of the routine STPS-II allowed us to study the Hg atom penetration into bulk Pt through the q_{Hg} vs $t_h^{1/2}$ plots (Fig. 10). For this purpose, first the q_{Hg} ML charge density ($q_{Hg,ML}$) on the cs-Pt electrode was evaluated taking into account the crystallographic radii of the species involved ($r_{Pt} = 0.139$ nm and $r_m = r_{Hg} = 0.157$ nm) [42, 43] and the surface excess (Γ_{max}), related to the maximum amount of Hg that might be deposited on a Pt electrode as follows, $\Gamma_{max} = \Delta q_{max}/zF = 2.17 \times 10^{-9}$ mol cm^{-2}; and $\Gamma_m = \Gamma_{max}(r_{Pt}/r_{Hg})^2 = 1.7 \times 10^{-9}$ mol $cm^{-2} = 164\ \mu C\ cm^{-2}$. Accordingly, for the Hg ML, $q_{Hg,ML} = 328\ \mu C\ cm^{-2}$.

Furthermore, the q_{Hg} vs $t_h^{1/2}$ linear behavior (Fig. 10) is obeyed from $q_{Hg} \cong 250\ \mu C\ cm^{-2} < q_{Hg,ML}$ to reach $q_{Hg} \gg q_{Hg,ML}$ values. Likewise, for $q_{Hg} \gg q_{Hg,ML}$, at a constant t_h, the higher q_{Hg} the lower E_h. The difference in q_{Hg} with respect to $q_{Hg,ML}$ can be attributed to the Hg atom penetration into bulk Pt.

3.3.2. *The formation of 2d and 3d Hg domains and Hg–Pt alloy at cs-Pt*. Runs were also made starting from a cs-Pt ($R = 70$ and $x = 10^{-3}$) under routine STPS-II for $E_{sc} = 0.02$ V, $E_{sa} = 1.55$ V, $v = 0.1\ V\ s^{-1}$, $E_h = 0.55$ V and $t_h = 10$ min. Subsequently, the Hg-covered cs-Pt electrode was transferred to a cell containing aqueous 0.5 M $HClO_4$ and then the routine RTPS-I was applied for $E_{sc} = 0.02$ V, $E_{sa} = 1.55$ V and $v = 0.1\ V\ s^{-1}$ (Fig. 11) paying special attention to the 1st, 2nd and 3rd successive voltammograms.

The first voltammogram (Fig. 11(a)) shows the stripping of bulk Hg to Hg(I) species appearing as a broad current peak at 0.78 V, followed by a current plateau extending from 1.22 V to 1.35 V related to the stripping of 2d Hg to Hg(II) species, and a large current peak at 1.51 V due to the anodic stripping of Hg to Hg(II) species from the Pt–Hg alloy. The reverse scan exhibits two current peaks, at 0.673 V and 0.345 V. The former peak exhibits the same features as those of the polarographic electroreduction peak of the Hg(I) to Hg(0) reaction on Hg [40, 41]. Then, initially the electrode behaved as a Hg-atom fully covered Pt electrode.

The second voltammogram (Fig. 11(a)) shows a decrease in the anodic stripping charge related to both the Hg bulk and Hg–Pt alloy, whereas the anodic charge of 2d Hg is increased. In this case, the

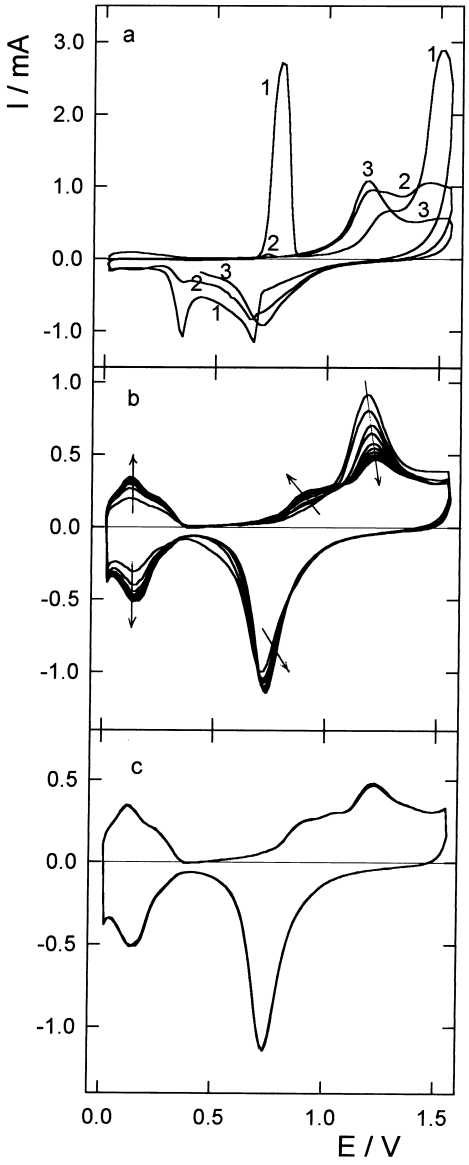

Fig. 11. Routine RTPS-I applied for $E_{sc} = 0.02$ V, $E_{sa} = 1.55$ V and $v = 0.1\ V\ s^{-1}$ to a cs-Pt electrode ($R = 70$ and $x = 10^{-3}$) previously subjected to routine STPS-II for $E_{sc} = 0.02$ V, $E_{sa} = 1.55$ V, $v = 0.1\ V\ s^{-1}$, $E_h = 0.55$ V and $t_h = 10$ min and subsequently transferring the Hg covered cs-Pt electrode to a cell containing aqueous 0.5 M $HClO_4$.

electrooxidation of both bulk Hg and Hg–Pt alloy is favoured, so that the electrode becomes principally covered by a quasi 2d Hg layer. Accordingly, the reverse scan tends to resemble that shown in the first voltammogram of Fig. 11(a), although the contribution of cathodic current peaks is considerably diminished.

The third voltammogram (Fig. 11(a)) shows the disappearance of the anodic stripping peak of bulk Hg, only a minor contribution of Hg–Pt alloying, and a maximum contribution of 2d Hg formation (current

peak at 1.18 V). Then, at this stage a fraction of the cs-Pt surface is already available for the H- and O-electrosorption reactions (Fig. 11(b)). A certain inhibition for these reactions remains due to the local concentration of Hg_2^{2+} ions produced in the 1st and 2nd electrooxidation scans. Subsequently, the cs-Pt electrode was transferred to another cell containing aqueous 0.5 M $HClO_4$ and the voltammogram resulting in this case tends to reproduce those features earlier described for the blank (Fig. 11(c)).

3.3.3. *The Hg_2^{2+}/H displacement reaction at cs-Pt.* Voltammograms resulting from cs-Pt under routine RTPS-I for $E_{sc} = 0.02$ V to $E_{sa} = 1.45$ V, $v = 0.02$ V s^{-1} and $10^{-4} \leqslant x \leqslant 10^{-3}$, after several hours in the solution under open circuit, reproduce the voltammetric features of the reversible Hg/Hg_2^{2+} and Hg/Hg^{2+} electrode reactions occurring either at the Hg electrode or at the cs-Pt electrode when the latter is entirely covered by Hg in aqueous 0.5 M $HClO_4$, as described above (Fig. 11(a)).

From these results it can be concluded that the spontaneous plating of Hg on cs-Pt at open circuit takes place, and that at constant Hg_2^{2+} ion concentration in the solution the immersion time required for cs-Pt to become entirely covered by a Hg film increases with R because of the diffusion of Hg_2^{2+} ions from the solution to the inner part of the cs-Pt structure. The formation of the Hg film involves a displacement reaction taking place at the void walls of the cs-Pt structure such as

$$2Pt(H) + Hg_2^{2+} = 2H^+ + 2Pt(Hg). \qquad (1)$$

Accordingly, the completion of this reaction implies that the open circuit potential reaches the value $E_{oc} = 0.652 \pm 0.010$ V, a figure which is very close to E_r as referred to in Section 3.2. In fact, the value of E_{oc} calculated from the reversible potentials [39, 40] corresponding to the Hg_2^{2+}/Hg and H^+/H electrodes for 10^{-4} M $Hg_2(NO_3)_2$ + 0.5 M $HClO_4$ is $E_{oc} = 0.656$ V. Therefore, in this respect, the behaviour of cs-Pt in Hg_2^{2+}-ion containing solutions is similar to that which has already been reported for cs-Pt electrodes in acid solutions containing Ag^+ ions [20].

4. DISCUSSION

4.1. Non-equilibrium Hg electrodeposits on cs-Pt

For those systems in which the metal–substrate (M–S) interaction exceeds the metal–metal (M–M) binding energy, the early stages of M electrodeposition can produce either a complete M–S domain followed by the 3d growth of bulk M, as predicted by the Stranski–Krastanov model or a layer by layer growth as predicted by the Frank-van der Merwe model under thermodynamic equilibrium. Otherwise, when the M–M interaction is stronger than the M–S interaction, the growth of incomplete M–S domains proceeds as predicted by the Volmer–Weber model before the complete surface coverage has been reached [10, 14, 19, 46, 50–57]. When the electrodeposition of M occurs on a well-defined, smooth S for a low potential scanning rate under the Stranski–Krastanov mechanism, the M–S deposit approaches equilibrium and then a complete M–S monolayer is produced before M–M domains begin to be formed, as in the case of Hg electrodeposition on smooth Pt. In contrast, when the electrodeposition of M takes place on an irregular substrate at either a moderate or a relatively fast potential scan, an inhomogeneous deposit involving incomplete M–S and M–M domains under non-equilibrium conditions is produced [20, 21, 23, 25, 28]. This implies that driving forces for M–S and M–M surface rearrangements to achieve equilibrium are present [25, 48]. The enhancement of a non-equilibrium situation at the irregular substrate, as is the case of cs-Pt, can be accomplished by an appropriate selection of both the electrode topography, and the potential or current perturbation conditions applied to the system and, to some extent, the solution composition. Voltammetric data on Hg electrodeposition on cs-Pt for given values of R, v and x, are consistent with a rearrangement in the Hg deposit in which 2d Hg–Pt domains are produced at the expense of 3d Hg–Hg domains.

For the discussion of this surface process, it is necessary to consider first in some detail the cs-Pt structure in contact with the aqueous solution. Assuming that each void at the cs-Pt, as derived from STM imaging (Fig. 2), can be approached as a quasi-cylindrical space, for $R = 30$, the average volume of the intercolumnar void $\langle v \rangle$, considering an average void diameter $\langle d \rangle \approx 10^{-6}$ cm and average void height $\langle h \rangle \approx 3 \times 10^{-5}$ cm, is $\langle v \rangle \approx 5 \times 10^{-17}$ cm^3. Accordingly, the average void wall area results in $\langle A \rangle \approx 10^{-12}$ cm^2. Otherwise, for $x = 10^{-3}$, the initial average number of Hg_2^{2+} ions at the void volume is $\langle N(Hg_2^{2+}) \rangle \approx 10$ [23], a figure which is much lower than $\langle N(Hg) \rangle \approx 10^3$, the average number of Hg atoms required to produce a ML coverage over the entire void wall. Therefore, from these figures it can be concluded that taking into account the relatively high exchange current density for the Hg_2^{2+}/Hg electrode reaction ($j_0 \approx 0.8$ A cm^{-2}) [40], the relatively slow ionic diffusion of Hg_2^{2+} at voids (D $(Hg_2^{2+}) \approx 10^{-5}$ cm^2 s^{-1}), the nil concentration of Hg_2^{2+} ions at voids will be rapidly attained under relatively fast electrodeposition conditions involved in the voltammetric electroreduction scan.

The preceding analysis indicates that the mass transport controlled Hg electrodeposition at cs-Pt at $v > 0.05$ V s^{-1}, takes place mostly at column tips and depending whether $E > E_r$ or $E < E_r$, different types of Hg electrodeposition will be produced. Thus, for $E > E_r$, Hg electrodeposition at voids is almost completely hindered, leading in the time range of the voltammetric scan to a cs-Pt electrode only partially covered by 2d Hg–Pt domains. The Hg ML coverage will be approached when $E \Rightarrow E_r$. Conversely, for

$E < E_r$, Hg 3d domains at column tips on 2d Hg–Pt existing domains will be preferentially formed, leaving rather large uncovered Pt domains, particularly at void walls. In fact, the presence of these uncovered domains is reflected by the appearance of a voltammetric current usually assigned to H atom electroadsorption (Fig. 4(b), (c)). Accordingly, the Hg voltammetric electrodeposition on cs-Pt results in an heterogeneous electrode surface under non-equilibrium.

The Hg_2^{2+} ion electrodeposition on cs-Pt, under the above mentioned conditions, implies the overlapping of radial diffusion fields established around column tips. Due to the tip-to-tip distance a linear diffusion field is produced. Then, as the Hg electrodeposition proceeds, the Hg surface concentration gradient between Hg covered domains (tips) and uncovered Pt areas (voids) acts as the driving force for Hg surface diffusion. Similarly, the Hg concentration gradient existing between the cs-Pt surface and bulk Pt will assist Hg–Pt alloy formation.

The extent of both the Hg surface diffusion and Hg penetration into bulk Pt depends on the Hg–Pt, Hg–Hg and Pt–Pt bond strength which determines to some extent the easiness of Hg atom displacement at the Pt surface and in bulk Pt [25]. For Hg atoms on the Pt surface, the balance between the very low heat of sublimation of Hg ($\Delta H_s = 14.5$ kcal/mol) [52] and the relatively high Hg–Pt binding energy (BE = 0.4 eV) [14] suggest that Hg adatoms can be considered as mobile species on the Pt surface. Furthermore, this characteristic of Hg adatoms on Pt and the trend of Hg to form Pt–Hg alloys with a rather high decomposition temperature [8, 11, 12, 43] favour Hg penetration into bulk Pt.

4.2. Kinetics and likely mechanism of Hg atom surface diffusion and penetration into bulk Pt

The penetration of Hg into bulk Pt can be described as the result from at least two distinguishable steps, namely, Hg atom shift to a position underlying the first layer of Pt atoms by a place exchange mechanism, and Hg penetration into bulk Pt, the rate of the first step being determined by the slowest mobile surface atom [24, 44, 45, 48, 49, 51, 52].

The penetration of Hg into bulk Pt should involve the inward shift of Hg atoms underlying the first layer of Pt atoms to attain the maximum Hg coordination number in the Pt lattice. This displacement of Hg atoms implies the creation of holes in bulk Pt to allow the Hg atom penetration [49–52]. The driving force for the Hg diffusion into bulk Pt is related to the chemical potential gradient of Hg built up between the Hg deposit and bulk Pt. This situation is similar to that extensively described for the underpotential alloy formation in the system Ag(*hkl*)/Cd^{2+} [45].

The diffusion coefficient of Hg into bulk Pt ($D_{Hg,Pt}$) can be roughly estimated from the anodic stripping charge of the Hg–Pt alloy after surface Hg has been oxidised (see also Section 3.3), using the Einstein–Smoluchowski equation $(\Delta x)^2 = D_{Hg,Pt}\, t$, where Δx is the thickness of the surface alloy at given holding potential and time. The calculation of Δx requires data on the mole fraction (x_{Hg}) and the density ($\rho_{Hg,Pt}$) of the surface alloy. According to previous works [6] the stoichiometry of the subsurface Pt–Hg alloy changes from $PtHg_2$ when a second monolayer of Hg is completely deposited, to the likely stoichiometry $PtHg_4$ when more than two surface monolayers of Hg are deposited.

Based upon the preceding approach, for $t_h = 600$ s and $E_h = 0.6$ V, a mean value of $\Delta q_{Hg}/F \cong 1 \times 10^{-8}$ mol cm^{-2} for the overall amount of Hg deposited is found (Fig. 10(c), (d)), which corresponds to a thickness of about $\Delta x \cong 1 \times 10^{-7}$ cm assuming a homogeneous phase ($PtHg_2$) of $x_{Hg} \cong 0.67$, and a density $\rho_{Hg,Pt} = 16.2$ g cm^{-3} [43]. From these data it results in $D_{Hg,Pt} \cong 2 \times 10^{-17}$ cm^2 s^{-1}, a figure close to values of $D_{Hg,Pt}$ previously reported for Hg diffusion into polycrystalline smooth Pt [10], and also of the same order of magnitude as those reported for the diffusion of other metal atoms into solid metal lattices [44–48]. It should be noted that the diffusion coefficient of Hg into bulk Pt under the electrochemical conditions described in this work is several order of magnitude smaller than the surface diffusion coefficient of Hg atoms calculated by Gojstein equation [58].

Finally, it is worth mentioning that the q_{Hg} vs $t_h^{1/2}$ plots involve an induction time t_i for the development of the Hg–Pt alloy (Fig. 10(c), (d)). The value of t_i, which decreases as E_h is diminished as should be expected when the value of q_{Hg} is increased, can be related to the time required to reach a threshold Hg atom surface coverage close to 0.66 for the penetration of Hg into Pt.

ACKNOWLEDGEMENTS

This work was financially supported by CONICET (Consejo Nacional de Investigaciones Científicas y Técnicas) and CIC (Comisión de Investigaciones Científicas de la Pcia. de Bs. As), Argentina.

REFERENCES

1. B. J. Bowles, *Nature* **212,** 1456 (1966).
2. A. I. Hartley, A. G. Hiebert and J. A. Cox, *J. Electroanal. Chem.* **17,** 81 (1968).
3. G. D. Robbins and C. G. Enke, *J. Electroanal. Chem.* **23,** 343 (1969).
4. L. Ramaley, R. L. Brubaker and C. G. Enke, *Anal. Chem.* **35,** 1088 (1968).
5. S. Bruckenstein and M. Z. Hassan, *Anal. Chem.* **43,** 928 (1971).
6. M. Z. Hassan, D. F. Untereker and S. Bruckenstein, *J. Electroanal. Chem.* **42,** 161 (1973) and references therein.
7. M. Stuliková, *J. Electroanal. Chem.* **48,** 33 (1973).

8. I. N. Plaksin and N. A. Suvorovskaya, *Acta Physicochim. URSS* **13,** 83 (1940); *C. R. Acad. Sci.* **27,** 460 (1940); *Zh. Fiz. Khim.* **15,** 978 (1941); *Izv. Zakt. Platiny Akad. Nauk. SSSR* **18,** 67 (1945).
9. L. A. Schadewald, T. R. Lindstrom, W. Hussein, E. E. Evenson and D. C. Johnson, *J. Electrochem. Soc.* **131,** 1583 (1984).
10. R. C. Salvarezza, D. V. Vásquez Moll, M. C. Giordano and A. J. Arvia, *J. Electroanal. Chem.* **213,** 301 (1986); R. C. Salvarezza and A. J. Arvia, *Electrochim. Acta* **33,** 1031 (1988).
11. S. Affrossman and J. Paton, *Soc. Chem. Ind. Lond.* **28,** 151 (1968).
12. S. Affrossman and W. G. Erskine, *Trans. Faraday Soc.* **62,** 2922 (1966).
13. S. Affrossman, W. G. Erskine and J. Paton, *Trans. Faraday Soc.* **64,** 2856 (1967).
14. D. M. Kolb, in *Advances in Electrochemistry and Electrochemical Engineering*, Vol 11, (Edited by H. Gerischer and C. Tobias), Wiley, New York (1978).
15. R. Adzic, in *Advances in Electrochemistry and Electrochemical Engineering*, Vol 13, (Edited by H. Gerischer and C. Tobias), Wiley, New York (1984).
16. G. Kokkinidis, *J. Electroanal. Chem.* **201,** 217 (1986).
17. S. Szabó, *Intern. Rev. Phys. Chem.* **10,** 207 (1991).
18. M. Breiter, *Electrochim. Acta* **34,** 1119 (1989).
19. D. Margheritis, R. C. Salvarezza, M. C. Giordano and A. J. Arvia, *J. Electroanal. Chem.* **229,** 327 (1989).
20. M. E. Martins, R. C. Salvarezza and A. J. Arvia, *Electrochim. Acta* **36,** 1617 (1991).
21. M. E. Martins, R. C. Salvarezza and A. J. Arvia, *J. Electrochem. Soc.* **138,** 2509 (1991).
22. K. Sashita, N. Furuya and K. Itaya, *J. Electroanal. Chem.* **316,** 361 (1991).
23. M. E. Martins, R. C. Salvarezza and A. J. Arvia, *Electrochim. Acta* **37,** 2203 (1992).
24. P. Ocón, P. Herrasti, C. Palacio, M. E. Vela, R. C. Salvarezza, L. Vázquez and A. J Arvia, *J. Electroanal. Chem.* **357,** 339 (1993).
25. M. E. Martins, R. C. Salvarezza and A. J. Arvia, *Electrochim. Acta* **41,** 2441 (1996).
26. J. M. Gómez Rodríguez, A. M. Baró, L. Vázquez, J. M. Vara, R. C. Salvarezza and A. J. Arvia, *J. Phys. Chem.* **96,** 347 (1992).
27. A. Chialvo, W. E. Triaca and A. J. Arvia. *J. Electranal. Chem.* **146,** 93 (1983).
28. A. E. Bolzán, A. M. Castro Luna, A. Visintín and A. J. Arvia, *Electrochim. Acta* **33,** 1743 (1988).
29. L. Vázquez, J. Gómez, A. M. Baró, N. García, M. L. Marcos, J. González Velasco, J. M. Vara, A. J. Arvia, J. Presa, A. García and M. Aguilar, *J. Am. Chem. Soc.* **109,** 1731 (1987).
30. C. Alonso, R. C. Salvarezza, J. M. Vara, A. J. Arvia, L. Vázquez, A. Bartolomé and A. M. Baró, *J. Electrochem. Soc.* **137,** 2161 (1990).
31. J. Zerbino, C. L. Perdriel and A. J. Arvia, *Thin Solid Films* **232,** 63 (1993).
32. R. O. Lezna, N. R. de Tacconi, C. L. Perdriel and A. J. Arvia, *Proc. Symp. Electrochem. Soc. on Electrode Materials* (Edited by S. Srinivasan, S. Wagner and H. Wroblova), Vol. 87-12, p. 31, The Electrochemical Society, Pennington, N.J. (1987).
33. A. M. Castro Luna, M. C. Giordano and A. J. Arvia, *J. Electroanal. Chem.* **259,** 173 (1989).
34. A. M. Castro Luna, A. E. Bolzán, M. L. F. de Mele and A. J. Arvia, *Pure and Appl. Chem.* **63,** 1599 (1991).
35. M. C. Arévalo, A. M. Castro Luna, A. A. Arévalo and A. J. Arvia, *J. Electroanal. Chem.* **330,** 595 (1992).
36. M. M. Gómez, L. Vázquez, R. C. Salvarezza, J. M. Vara and A. J. Arvia, *J. Electroanal. Chem.* **125,** 317 (1991).
37. S. G. Real, J. R. Vilche and A. J. Arvia, *J. Electroanal. Chem.* **341,** 181 (1992).
38. S. Trassati and O. A. Petrii. *Pure Appl. Chem.* **63,** 711 (1991).
39. A. J. Bard, R. Parsons and J. Jordan (Eds.), *Standard Potentials in Aqueous Solution*, International Union of Pure and Applied Chemistry, Dekker, New York (1985).
40. *Encyclopedia of the Electrochemistry of the Elements* (Edited by A. J. Bard), Vol IX.A.1, Marcel Dekker, New York (1982).
41. I. M. Kolthoff and C. S. M. Miller, *J. Am. Chem. Soc.* **63,** 2732 (1941).
42. *Handbook of Chemistry and Physics*, 73rd. edition, (D. R. Lide, editor), CRC Press, Boca Ratón (1993).
43. W. E. Pearson, *A Handbook of Lattice Spacings and Structures of Metals and Alloys*, Pergamon Press, Oxford (1964).
44. E. Schmidt, M. Christen and P. Beyeler, *J. Electroanal. Chem.* **42,** 275 (1973).
45. H. Bort, K. Jüttner, W. J. Lorenz and G. Staikov, *Electrochim. Acta* **28,** 993 (1983).
46. D. C. Alonzo and B. R. Scharifker, *J. Electroanal. Chem.* **274,** 167 (1989).
47. D. Aberdam, C. Salem, R. Durand and R. Faure, *Surf. Sci.* **239,** 71 (1990).
48. M. E. Martins, A. Hernández Creus, R. C. Salvarezza and A. J. Arvia, *J. Electroanal. Chem.* **375,** 141 (1994).
49. A. J. E. Welch in W. E. Garner (Ed.), *Chemistry of the Solid State*, Ch 12, Butterworths, London (1955).
50. J. Bénard, *Adsorption on Metal Surfaces*. Studies in Surface Science and Catalysis, Vol 13, Wiley-Elsevier, Amsterdam (1983).
51. W. Jost, *Diffusion in Solids*, *Liquids*, *Gases*, Academic Press, New York (1955).
52. F. Seitz, *The Modern Theory of Solids*, McGraw-Hill, New York (1940).
53. H. Bort, K. Jüttner, W. J. Lorenz, G. Staikov and B. Budevski, *Electrochim. Acta* **28,** 985 (1983) and references therein.
54. T. Chierchie, C. Mayer, H. Bort, K. Jüttner and W. J. Lorenz, *J. Electroanal. Chem.* **191,** 401 (1985).
55. T. Vitanov, A. Popov, G. Staikov, E. Budevski, W. J. Lorenz and E. Schmidt, *Electrochim. Acta* **31,** 981 (1986).
56. W. J. Lorenz, L. M. Gassa, U. Schmidt, W. Obretenov, G. Staikov, V. Bostanov and E. Budevski, *Electrochim. Acta* **37,** 2173 (1992).
57. W. Obretenov, W. J. Lorenz, U. Schmidt, G. Staikov, E. Budevski, D. Carnal, U. Müller, H. Siegenthaler and E. Schmidt, *J. Electrochem. Soc.* **140,** 692 (1993) and references therein.
58. N. A. Gojstein, J. J. Bruke, N. L. Reed and V. Weiss (Eds.), *Surfaces and Interfaces I*, p. 271, Syracuse University Press, Syracuse, New York (1967).